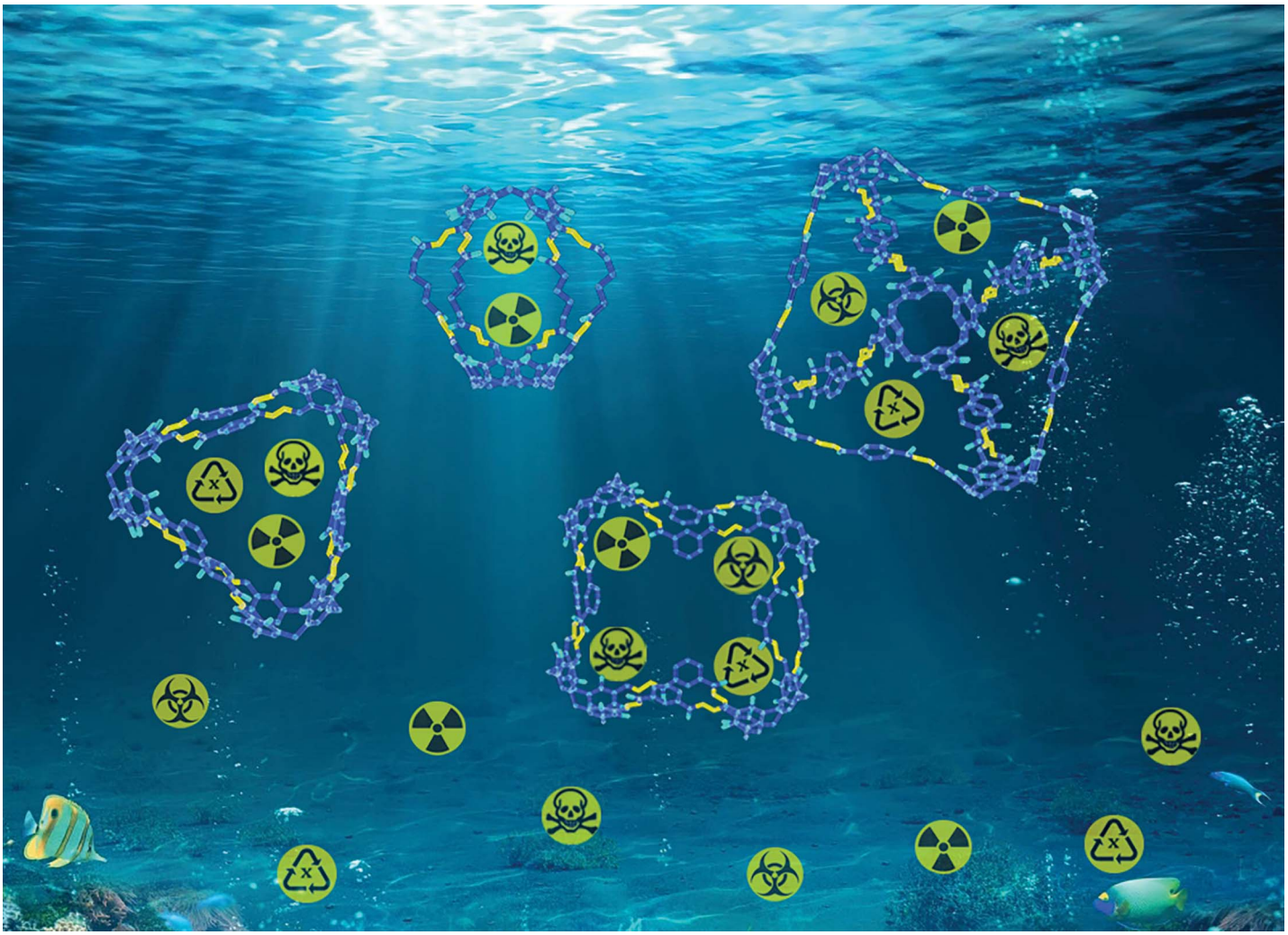

Showcasing research from Professor Daqiang Yuan's laboratory, Fujian Institute of Research on the Structure of Matter, Chinese Academy of Sciences, Fuzhou, China.

Water-stable hydrazone-linked porous organic cages

A convenient method for constructing water-stable hydrazone-linked porous organic cages with tunable structures from [2+4] lantern, [3+6] triangular prism, unprecedented [4+8] square prism, to extra-large [6+12] octahedron has been reported. They are fully determined by single-crystal X-ray crystallography and exhibit tunable window diameters and cavity volumes from 5.4 to 11.1 nm and 580 to 6800 Å^3, respectively. Moreover, they can be used as robust absorbents for effective removal of various pollutants from water, including radionuclide waste, toxic heavy metal ions, and organic micropollutants.

As featured in:

See Kongzhao Su, Daqiang Yuan *et al.*, *Chem. Sci.*, 2021, **12**, 13307.

ROYAL SOCIETY OF CHEMISTRY

rsc.li/chemical-science

Registered charity number: 207890

Chemical Science

ROYAL SOCIETY OF CHEMISTRY

EDGE ARTICLE

View Article Online
View Journal | View Issue

Open Access Article. Published on 23 shtator 2021. Downloaded on 12.8.2025 2:07:18 e pasdites.
This article is licensed under a Creative Commons Attribution-NonCommercial 3.0 Unported Licence.

Check for updates

Cite this: *Chem. Sci.*, 2021, **12**, 13307

All publication charges for this article have been paid for by the Royal Society of Chemistry

Water-stable hydrazone-linked porous organic cages†

Miao Yang,[ab] Fenglei Qiu,[ad] El-Sayed M. El-Sayed,[ace] Wenjing Wang,[ac] Shunfu Du,[ad] Kongzhao Su *[ac] and Daqiang Yuan *[ac]

Although porous organic cages (POCs), particularly imine-linked (C=N) ones, have advanced significantly over the last few decades, the reversible nature of imine linkages makes them prone to hydrolysis and structural collapse, severely limiting their applications under moist or water conditions. Herein, seven water-stable hydrazone-linked (C=N–N) POCs are prepared through a simple coupling of the same supramolecular tetraformylresorcin[4]arene cavitand with different dihydrazide linkers. Their structures are all determined by single-crystal X-ray crystallography, demonstrating rich structural diversity from the [2 + 4] lantern, [3 + 6] triangular prism, and unprecedented [4 + 8] square prism to the extra-large [6 + 12] octahedron. In addition, they respectively exhibit tunable window diameters and cavity volumes ranging from about 5.4 to 11.1 nm and 580 to 6800 Å^3. Moreover, their application in the water environment for pollutant removal was explored, indicating that they can effectively eliminate various types of contaminants from water, including radionuclide waste, toxic heavy metal ions, and organic micropollutants. This work demonstrates a convenient method for rationally constructing versatile robust POCs and presents their great application potentialities in water medium.

Received 17th August 2021
Accepted 23rd September 2021

DOI: 10.1039/d1sc04531h

rsc.li/chemical-science

Introduction

The burgeoning porous organic cages (POCs),[1–6] constructed by covalently linking organic building blocks to form zero-dimensional (0D) discrete molecules with designable hollow cavities, are complementary to the well-developed covalent organic frameworks (COFs),[7–9] also built from organic building blocks but with infinite extended 2D or 3D structures. Due to their discrete nature, POCs exhibit numerous unique properties, including solubility, processing, functionalization, and regeneration in solution,[10,11] and have recently garnered considerable attention. Since the first elegant report in 2009 by Cooper *et al.*,[12] many POCs with different shapes and properties have been reported over the last decade, but they are mostly linked by dynamic and reversible imine (C=N) and B–O bonds.[13–31] Such POC types are prone to hydrolysis and skeleton collapse upon exposure to water, making them nonporous in nature and severely limiting their applications in a water environment. Four strategies have been validated thus far for constructing water-stable POCs: (1) using irreversible C–C or C–O bonds;[32–35] (2) introducing ethynylene linkages (C≡C);[36–39] (3) transforming labile C=N bonds to chemically robust amide (C–N) bonds by post-modification or an *in situ* reduction method;[40–44] and (4) introducing alkyl groups into aldehydes for protecting POCs' C=N bonds by steric and hydrophobic control.[45–47] Because the abovementioned methods for preparing water-stable POCs frequently encounter difficulties such as tedious multistep organic synthesis with low product yield, using expensive catalysts, and difficulty in number and structural diversity extension, synthesizing water-stable POCs using a cost-effective and straightforward procedure is highly desirable.

The hydrazone bond (C=N–N) is formed when hydrazine- or hydrazide-containing compounds react with aldehydes and can be regarded as N-substituted imine derivatives. Notably, such N-substitution makes hydrazones robust enough against hydrolysis compared to their parent imines under water conditions because the adjacent N atom's lone pair electrons can delocalize into a C=N bond and make it less electrophilic and hence more stable.[48] Until now, many robust hydrazone-linked COFs *via* integrating different hydrazine- and aldehyde-containing building blocks have been prepared and demonstrated applications under moist and water conditions, such as water pollutant removal, proton conduction, energy production/

[a]State Key Laboratory of Structural Chemistry, Fujian Institute of Research on the Structure of Matter, Chinese Academy of Sciences, Fuzhou, 350002, China. E-mail: skz@fjirsm.ac.cn; ydq@fjirsm.ac.cn

[b]College of Chemistry and Materials Science, Fujian Normal University, Fuzhou, 350007, China

[c]University of the Chinese Academy of Sciences, Beijing, 100049, China

[d]College of Chemistry, Fuzhou University, Fuzhou 350116, China

[e]Chemical Refining Laboratory, Refining Department, Egyptian Petroleum Research Institute, Nasr City, 11727, Egypt

† Electronic supplementary information (ESI) available: For ESI and crystallographic data in CIF or other electronic format. CCDC 2097226–2097232. For ESI and crystallographic data in CIF or other electronic format see DOI: 10.1039/d1sc04531h

© 2021 The Author(s). Published by the Royal Society of Chemistry

Open Access Article. Published on 23 shtator 2021. Downloaded on 12.8.2025 2:07:18 e pasdites.
This article is licensed under a Creative Commons Attribution-NonCommercial 3.0 Unported Licence.

storage, drug delivery, and so on.[49–54] However, no hydrazone-linked COF has been characterized using single-crystal X-ray diffraction (SCXRD). In contrast, exploring discrete hydrazone-linked organic cage compounds remains in its initial stage, regardless of their number or applications. Although hydrazone-linked organic cages have the advantage of solving their structures by SCXRD, they still face significant difficulties in determining their structures due to weak crystal diffraction, particularly large ones due to the absence of heavy atoms in the molecular structure. To the best of our knowledge, only four hydrazone-linked organic cage structures are solved by SCXRD, and none of their cavity diameters is more than 2.5 nm.[55–58] Both indexes are much lower than those of imine-linked cages with numerous crystals characterized by SCXRD and a cavity diameter up to 4.3 nm.[59] Moreover, none of the reported hydrazone-linked organic cages has been explored as a porous molecular solid for practical applications.

Calix[4]resorcinarene (C4RA), a macrocyclic molecule with an intrinsic cavity and eight polar upper-rim phenolic groups, has been demonstrated as an excellent building block to construct cage compounds with rich cavity sizes and shapes, which can encapsulate guests from small gases to large molecules.[60–65] Our group is particularly interested in preparing new C4RA-based porous materials and their applications in energy and environmental aspects.[66–70] In this work, seven new water-robust POCs with specific crystal structures, including the [2 + 4] lantern, [3 + 6] triangular prism, unprecedented [4 + 8] square prism, and gigantic [6 + 12] octahedron, are constructed from the same concave-shaped tetraformyl-functionalized C4RA (C4RACHO) scaffold and different dihydrazide linkers with only *N*,*N*-dimethylformamide (DMF) as solvent (Scheme 1). Although it has remained challenging to develop a general synthetic method for systematic preparation of versatile POC crystals, this work suggests that C4RACHO can be a good candidate to reach this goal. Moreover, their application in removing water contaminants has been explored.

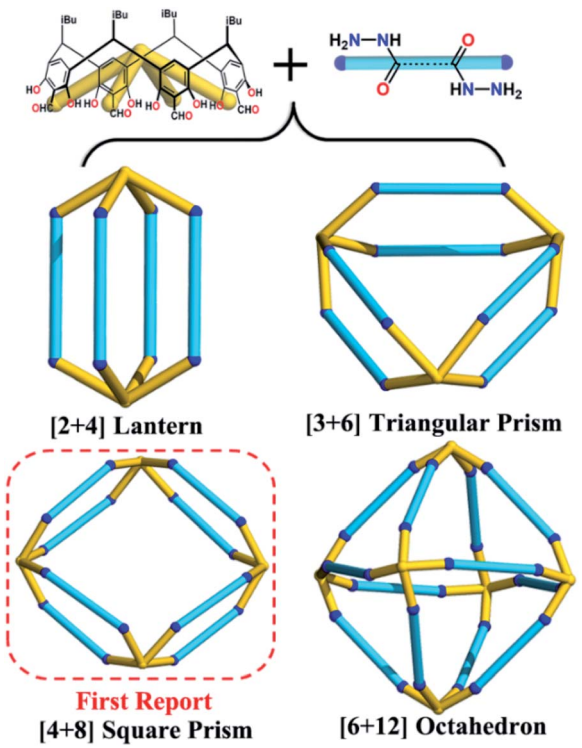

Scheme 1 Self-assembly of organic cages constructed from the tetratopic C4RACHO cavitand and dihydrazide linkers.

Results and discussion

Seven hydrazone-linked POCs with four types of assembly modes can be obtained from hydrazone coupling between C4RACHO (1 eq.) and different dihydrazides (2 eq.), varying from flexible alkanedihydrazide and V-shaped *m*-phthaloyldihydrazide to linear terephthalohydrazide in DMF at 100 °C. Initially, using propanedioyl dihydrazide isolated a [2 + 4] lantern-shaped organic cage, namely **HPOC-101**, constructed from two C4RACHO as vertexes and four propanedioyl dihydrazide linkers as pillars (Fig. 1 and S1†). SCXRD analysis suggests that **HPOC-101** crystallizes in a triclinic system with a space group of *P*-1, exhibiting two cage molecules per unit cell and eight DMF solvent molecules. These DMF molecules are all located in the cage interstices (Fig. S2†). **HPOC-101** consists of one central lantern-shaped cavity and four rhombus-shaped windows, which remarkably resemble our previously reported amine-linked organic cage constructed from propane-1,3-diamine. Its cavity height is about 1.34 nm (measured between

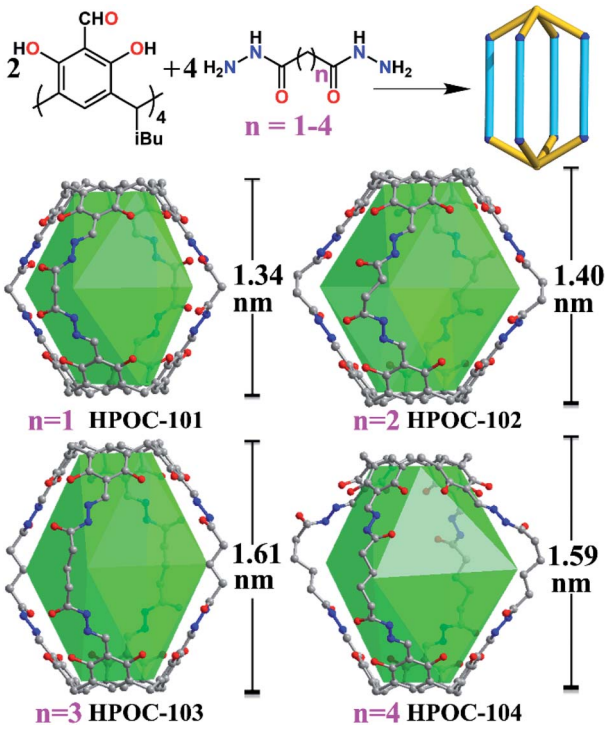

Fig. 1 Schematic illustration of the assembly of [2 + 4] lanterns *via* hydrazone coupling of C4RACHO and alkanedihydrazides, along with their single-crystal X-ray structures and inner cavity heights. Carbon is grey, oxygen is red, and nitrogen is blue. The hydrogen atoms and *iso*-butyl groups are omitted for clarity.

 © 2021 The Author(s). Published by the Royal Society of Chemistry

Open Access Article. Published on 23 shtator 2021. Downloaded on 12.8.2025 2:07:18 e pasdites.
This article is licensed under a Creative Commons Attribution-NonCommercial 3.0 Unported Licence.

bottom centers of opposite C4RA units), and its calculated volume by Voidoo is 582 Å^3.[71,72] The diagonals of a rhombus-shaped window in **HPOC-101** are approximately 1.3 × 1.5 nm (measured between the opposite bridge and methylene carbon of C4RA units and dihydrazide linkers, respectively), which can be penetrated by a sphere with a diameter of 5.42 Å calculated from Pywindow.[73] Our previous work demonstrated that POCs constructed from C4RACHO and flexible alkanediamines exhibit an odd–even effect, in which C4RA-based POCs derived from odd diamines (having an odd number of methylene groups) are conformationally eclipsed. In contrast, those constructed from even diamines adopt a gauche conformation.[67] Our primary motivation was to determine whether the odd–even effect is retained in the alkanedihydrazide system, and thus butanedioyl, pentanedioyl, and hexanedioyl dihydrazides with increasing methylene number were chosen for constructing **HPOC-102**, **HPOC-103**, and **HPOC-104**, respectively (Fig. 1). Notably, these four flexible alkanedihydrazide linkers have not been previously employed in constructing organic cages. SCXRD measurements reveal that they exhibit the same [2 + 4] assembly modes as **HPOC-101**. Except for **HPOC-104**, which crystallizes in the monoclinic *C*2/*c* space group, the remaining **HPOC-102** and **HPOC-103** both crystallize in the triclinic space group *P*-1, the same as **HPOC-101**. In the extended structures of **HPOC-102** to **HPOC-104**, their cage cavities and/or interstices are filled with DMF solvent molecules (Fig. S3–S5†). Further inspection of their crystal structures demonstrated that oxygen atoms of alkanedihydrazides from **HPOC-101** to **HPOC-103** are on the same side, while those in **HPOC-104** are on the opposite side. Such difference leads to two calix[4]resorcinarene units in **HPOC-104** with a gauche conformation, while the other three cages adopt eclipsed conformations (Fig. S9†). Accordingly, **HPOC-101** to **HPOC-103** can be regarded as regular lanterns, whereas **HPOC-104** is a distorted lantern. By increasing the pillar length, the inner cavity height and cavity volumes from **HPOC-101** to **HPOC-103** gradually increased from 1.34 to 1.61 nm and 582 to 833 Å^3 (Table S3†), respectively. Given the distortion, the cavity height and volume of **HPOC-104** are 1.59 nm and 859 Å^3, which are close to those of **HPOC-103**. Moreover, the related window diameters for **HPOC-102**, **HPOC-103**, and **HPOC-104** are 5.60, 6.32, and 6.60 Å, respectively.

Following that, using V-shaped *m*-phthaloyldihydrazide and C4RACHO unexpectedly afforded a mixture of block-shaped (**HPOC-201**) and rhombus-shaped (**HPOC-301**) crystal mixtures with a ratio of about 1 : 7 (Fig. S1†). Such a phenomenon has also been observed in other supramolecular macrocycles, metal–organic nanocages, and organic cage systems.[74–77] All attempts to control the assembly of these two cages by varying solvent and/or temperature were unsuccessful. SCXRD analysis indicates that the block-shaped crystal is a common [3 + 6] triangular prism assembled from three C4RACHO cavitands as faces and six *m*-phthaloyldihydrazide ligands as edges. On the other hand, the rhombus-shaped crystal possesses an unprecedented [4 + 8] square prism with four C4RACHO faces and eight *m*-phthaloyldihydrazide edges (Fig. 2). Both structures are significantly different from previously reported dimeric cages based on *m*-phthaloyldihydrazide, but methylene-bridged tetraformylresorcin[4]arene cavitands, demonstrating a slight change in the cavitand parent that largely influences the resulting cage shapes.[57] Moreover, the self-assembly of rigid 1,3-phenylenediamine and C4RACHO only affords the [3 + 6] triangular prism in our previous report,[67] indicating that increasing linker flexibility (in this case *m*-phthaloyldihydrazide compared to *m*-phenylenediamine) can be an effective way to increase organic cage structural diversity. SCXRD analysis reveals that both **HPOC-201** and **HPOC-301** are in the monoclinic space group *C*2/*c* with a large cavity and two windows. Close inspection of the structures revealed that all windows in **HPOC-201** are similar, but different in **HPOC-301**. Specifically, the three phenyl rings of *m*-phthaloyldihydrazide on each side of **HPOC-201** are oriented toward the vertical direction of the cavity (Fig. S10†). The four phenyl rings on one side of **HPOC-**

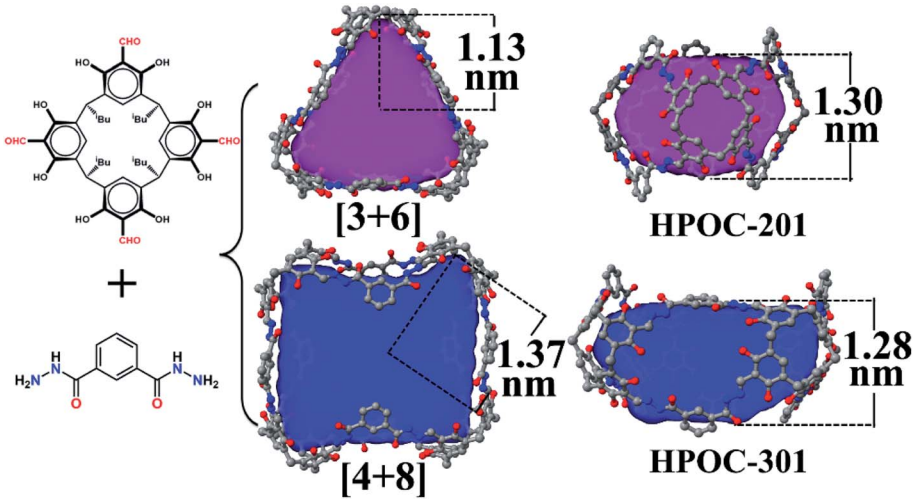

Fig. 2 Schematic illustration of the assembly of the [3 + 6] triangular prism and [4 + 8] square prism based on C4RACHO and the V-shaped *m*-phthaloyldihydrazide linker and their X-ray crystal structures. The hydrogen atoms and *iso*-butyl groups are omitted for clarity.

Open Access Article. Published on 23 shtator 2021. Downloaded on 12.8.2025 2:07:18 e pasdites.
This article is licensed under a Creative Commons Attribution-NonCommercial 3.0 Unported Licence.

301 are oriented toward the vertical direction of the cavity, while two opposite phenyl rings on the other side are oriented toward the horizontal direction (Fig. S11†). Moreover, numerous DMF molecules can be observed in cage cavities and interstices of **HPOC-201** (Fig. S6†). Notably, DMF guests could not be located in **HPOC-301** due to weak crystal diffraction, and thus their contribution has been subtracted from diffraction data using the SQUEEZE function of PLATON.[78] Moreover, cavity heights and volumes are 1.30 and 1.28 nm, and 1638 and 3098 Å^3 for **HPOC-201** and **HPOC-301**, respectively. The average maximum cavity radii of **HPOC-201** and **HPOC-301** are 1.13 and 1.37 nm (measured between the center of the cavity and bottom centers of C4RA units), respectively. The average length of trigonal and square windows is about 1.95 nm (measured between the neighboring bridge carbon of C4RA units) for **HPOC-201** and **HPOC-301**, which can be respectively penetrated by a sphere with a diameter of 9.66 and 11.13 Å calculated from Pywindow.

Finally, a gigantic octahedral [6 + 12] organic cage (**HPOC-401**) was obtained from the self-assembly of linear terephthalohydrazide and C4RACHO units (Fig. 3). SCXRD analysis reveals that **HPOC-401** exhibits a large asymmetric unit and belongs to the orthogonal space group *Pnnn* with six cage molecules per unit cell. Due to weak crystal diffraction, DMF solvent molecules in the cage cavity and interstice were also challenging to determine. Its molecular shape is similar to that of the reported organic cage constructed from the C4RACHO scaffold and *p*-phenylenediamine linkers. **HPOC-401** features an extra-large octahedral cavity and eight trigonal windows. Its calculated maximum cavity diameter (measured between bottom centers of opposite C4RA units) and volume are about 3.25 nm and 6800 Å^3, which are the largest in reported hydrazone-linked organic cages characterized by SCXRD. To date, the largest reported hydrazone-linked organic cage is a [3 + 3] RC4A-based cage constructed from three tetraformyl-functionalized RC4As and three tetrahydrazone-functionalized RC4As, containing an internal cavity with a maximum diameter of 2.12 nm and volume of about 1883 Å^3 calculated by Voidoo.[56] Moreover, the average length of the trigonal window is about 2.0 nm (measured between the neighboring bridge carbon of C4RA units), which is large enough to accommodate a molecule with a diameter of 9.51 nm.

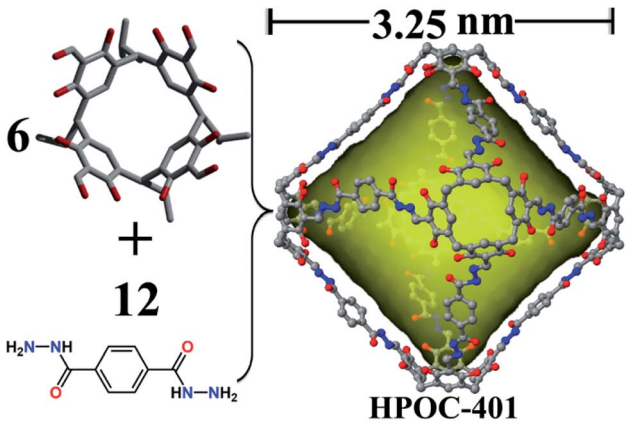

Fig. 3 Schematic illustration of the assembly of the [6 + 12] octahedron based on C4RACHO and the linear terephthalohydrazide linker and its X-ray crystal structure. The hydrogen atoms and *iso*-butyl groups are omitted for clarity.

The crystal data, window diameters, and cavity volumes for the abovementioned hydrazone-linked POCs are summarized in Table S3.† Apart from SCXRD data, the aforementioned hydrazone-linked C4RA-based POC samples were further characterized by Fourier-transform infrared spectroscopy (FT-IR), mass-spectrometry (MS), and proton nuclear magnetic resonance (^{1}H NMR) analytical measurements. FT-IR spectra of all POCs exhibit a characteristic C=N stretching around 1666 cm^{-1} (Fig. S12–S18†). ^{1}H NMR spectra do not show any characteristic peak of –CHO of C4RACHO; instead, they show peaks characteristic of H–C=N at about 8.6 ppm for [2 + 4] hydrazone-linked POCs and about 9.0 ppm for the remaining POCs (Fig. S19–S24†). Moreover, the observed *m*/*z* values of molecular ion peaks for each POC were consistent with their calculated molar masses (Fig. S25–S31†), demonstrating the presence of intact hydrazone-linked cages in solutions. Thermogravimetric analysis (TGA) reveals that POCs are thermally stable up to ~280 °C under nitrogen (N_2) gas (Fig. S32–S37†). In addition, their water stability was confirmed by measuring ^{1}H NMR spectra of POC samples being soaked in water for a week, and the unchanged signals indicate the robustness of cages in water (Fig. 4 inset and Fig. S20–S24†). Notably, these hydrazone-linked cage architectures remain intact following guest solvent removal because the above-mentioned FT-IR, MS, and ^{1}H NMR characterization studies are conducted on desolvated samples.

The porosity of cages was estimated using carbon dioxide (CO_2) sorption at 196 K, as they exhibit less significant N_2 sorption behavior at 77 K (Fig. S44–S49†), which is often observed in porous molecular organic crystals such as hydrogen-bonded organic frameworks (HOFs),[79,80] supramolecular organic frameworks (SOFs),[81,82] and POCs.[83,84] As displayed in Fig. 5 and Table S3,† CO_2 adsorption isotherms suggest that these hydrazone-linked POCs can adsorb a moderately high volume of CO_2 with capacities up to 234 cm^3 g^{-1} at 196 K and 760 mmHg. This value is comparable to those of other reported POC materials (PB-2, 265 cm^3 g^{-1}; Fe-PB, 225 cm^3 g^{-1}).[45,85] The calculated Brunauer–Emmett–Teller (BET) surface areas of cages are within the range of 373 to 563 m^2 g^{-1} (Table S3† and Fig. S50–S55†). Notably, these calculated surface areas do not match their cavity volumes, possibly due to the absence of proper connectivity between cavity voids, and/or due to cavity voids in the solid crystal packing being blocked by neighboring cages after desolvation (Fig. S38–S43†). Moreover, CO_2 and acetylene (C_2H_2) adsorptions of **HPOC-101** to **HPOC-104** at room temperature were also explored, affording C_2H_2 capacity from 31 to 47 cm^3 g^{-1} and CO_2 capacity from 24 to 33 cm^3 g^{-1} (Fig. 4c and S57–S59†). As they all prefer to adsorb C_2H_2 over CO_2, dynamic C_2H_2/CO_2 (50% : 50%) breakthrough experiments for **HPOC-102** and **HPOC-104** were performed (Fig. 4d and S60†). The experiments confirmed that cages could effectively separate the C_2H_2/CO_2 mixture, indicating their promising adsorption performance in C_2H_2/CO_2 separation. Moreover, **HPOC-102** and **HPOC-104** also represent the first two

 © 2021 The Author(s). Published by the Royal Society of Chemistry

Open Access Article. Published on 23 shtator 2021. Downloaded on 12.8.2025 2:07:18 e pasdites.
This article is licensed under a Creative Commons Attribution-NonCommercial 3.0 Unported Licence.

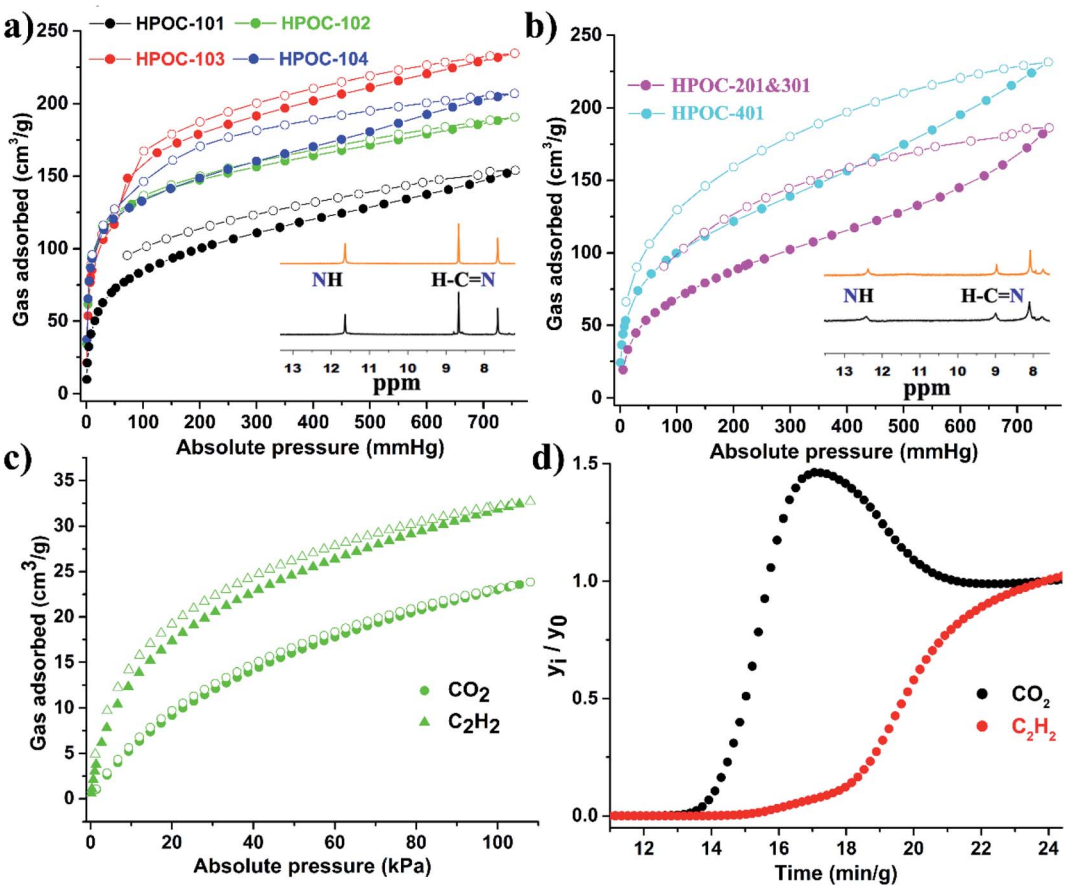

Fig. 4 (a and b) CO_2 sorption isotherms of hydrazone-linked POCs at 196 K and 760 mmHg. Insets a and b are water-stability tests of **HPOC-101** and **HPOC-401**, respectively. Black lines stand for pristine samples, whereas red lines represent the samples after being soaked in water for a week. (c) CO_2 and C_2H_2 adsorption isotherms of **HPOC-102** at 298 K. (d) Experimental breakthrough curves of an equimolar mixture of CO_2/C_2H_2 at 298 K and 1 bar over a packed bed of **HPOC-102**.

hydrazone-linked POC materials to realize C_2H_2/CO_2 gas separation.

Industrial and urban activities lead to various contaminants in water resources such as radionuclide waste, organic micropollutants, and toxic heavy metal ions that significantly exceed the standard limits, resulting in adverse effects on ecosystems and human health. Exploring and developing new materials for effective removal of these pollutants from contaminated water is critical to sustainable development of human society. Although metal–organic frameworks (MOFs), COFs, and porous organic polymers have recently been extensively studied for water pollutant removal,[86–88] investigating emerging POC materials for removing pollutants from aqueous solutions remains in its infancy. Hydrazone-linked POCs are better suited for this application due to their water-stable nature, porous nature, abundant multidentate N/O chelating sites, and π-rich cavities within their skeleton. Radioiodine (^{129}I and ^{131}I) was chosen as a model radionuclide waste pollutant because it is a major component of radionuclides and has recently attracted much public concern for wastewater leaks from the Fukushima nuclear disaster. To ensure safety, we used non-radioactive I_2 in KI water solution to mimic the radionuclide waste because iodine can easily exist as I_3^- ions by binding I^- to increase its water solubility. Adsorption of I_3^- was accomplished by immersing 3 mg desolvated POC samples in 6 mL KI/I_2 aqueous solution (0.337 mM), followed by stirring. The suspension was separated by filtration at different time intervals, and the solution was then detected using the UV-visible (UV-vis) spectrum by measuring the change of maximum adsorption of I_3^- at room temperature. All POC samples rapidly remove I_3^- within the initial 30 seconds and then increased slowly to achieve equilibrium at about 15 min with a removal rate >96% (Fig. 5a and S61–S66†). Notably, **HPOC-101** exhibits the fastest removal rate, the best removal efficiency, and the largest adsorption capacity (Table S5†), which might be ascribed to the fact that densities of chelating sites and RC4A cavities are higher than those of other cages, or its cavity is more suitable for accommodating the I_3^- guest. In addition, the maximum adsorption capacity of **HPOC-101** was investigated by soaking the sample in a highly concentrated KI/I_2 aqueous solution, and the experimental value was about 1305 mg g^{-1}, which fits well with the calculated value (1383 mg g^{-1} with correlation coefficient $R^2 = 0.9949$) based on the Langmuir model (Fig. S67 and Table S4†). X-ray photoelectron spectroscopy (XPS) measurement based on iodine-loaded **HPOC-101** suggests that iodine existed as both neutral I_2 and I_3^- forms (Fig. S68†), which might be due to the

Open Access Article. Published on 23 shtator 2021. Downloaded on 12.8.2025 2:07:18 e pasdites.
This article is licensed under a Creative Commons Attribution-NonCommercial 3.0 Unported Licence.

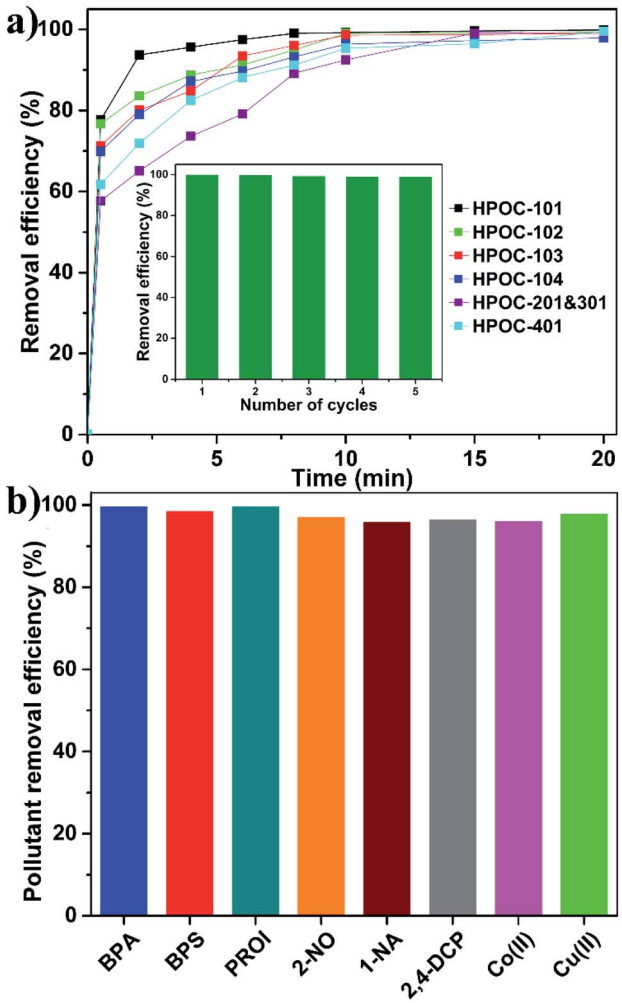

Fig. 5 (a) Time-dependent adsorption of aqueous I_3^- by hydrazone-linked POCs, inset: the recyclability of HPOC-101 for I_3^- removal. (b) Percentage removal efficiency of different water pollutants (0.1 mM) by HPOC-101 (0.5 mg mL^{-1}).

existence of charge transfer between iodine guests and the cage host, resulting in dynamic equilibrium between I_3^- ions and I_2 molecules in air, as confirmed by electron paramagnetic resonance (EPR, Fig. S69†). The recyclability of **HPOC-101** was then examined, suggesting that this adsorbent can keep high removal efficiency for at least five cycles (Fig. S5a† inset). These hydrazone-linked POCs represent the first examples of POC materials for iodine removal from water to the best of our knowledge. Moreover, the iodine vapor adsorption experiments of **HPOC-101** and **HPOC-401** have also been performed, which suggest that their maximum uptake capacities are about 220 wt% (Fig. S70 and S71†).

The excellent iodine removal ability combined with structural characteristics of **HPOC-101** could also eliminate other types of water pollutants, such as organic micropollutants and toxic heavy metal ions. Thus, organic micropollutants have been tested, including bisphenol A (BPA) and bisphenol S (BPS), as endocrine disruptors with greater environmental persistence from plastic; propranolol hydrochloride (PROI), as a beta-blocker used to treat hypertension from medical wastewater; and 2-naphthol (2-NO), 1-naphthyl amine (1-NA) and 2,4-dichlorophenol (2,4-DCP) as representatives for various simple aromatic pollutants, as well as Co^{2+} and Cu^{2+} toxic heavy metal ions. Interestingly, it was found that **HPOC-101** can effectively eliminate such water pollutants with removal efficiencies of >96% (Fig. 5b and S72–S77†), which are comparable to those of COF materials in organic micropollutant removal from water.[89–91] Notably, **HPOC-101** exhibits good efficiencies to remove metal ions, which can be ascribed to the tridentate O–N–O chelating sites in **HPOC-101** having good ability to complex with such metal ions; while the good efficiencies to remove organic micropollutants are mainly due to the host–guest interactions between the cage cavities and micropollutants, as well as the hydrogen bonding interactions between the N/O sites and micropollutants. Moreover, the efficiencies of **HPOC-401** to remove organic micropollutants were studied (Fig. S78–S82†), and its removal efficiencies under the same conditions are lower than those of **HPOC-101**. To the best of our knowledge, there is still no POC adsorbent with the ability to effectively eliminate these many kinds of water contaminants.

Conclusions

In summary, we have developed a general synthetic method using DMF as a solvent for constructing versatile hydrazone-linked POCs using the same tetraformylresorcin[4]arene cavitand and three different types of dihydrazide ligands, including flexible alkanedihydrazide, V-shaped *m*-phthaloyldihydrazide, and linear terephthalohydrazide based on the hydrazone coupling reaction. Five types of calix[4]-resorcinarene-based POCs, such as the [2 + 4] lantern (**HPOC-101** to **HPOC-103**), [2 + 4] distorted lantern (**HPOC-104**), [3 + 6] triangular prism (**HPOC-201**), [4 + 8] square prism (**HPOC-301**), and [6 + 12] octahedron (**HPOC-401**), have been obtained and characterized by SCXRD, FT-IR, MS, ^{1}H NMR, and TGA measurements. Their window diameters and cavity volumes can be precisely tuned from 5.4 to 11.1 Å and 580 to 6800 $Å^3$ using specific dihydrazide linkers. To the best of our knowledge, the square prism shape of **HPOC-301** has not been observed in organic cage systems, whereas **HPOC-401** is the largest hydrazone-linked organic cage with a unique X-ray crystal structure. Moreover, the abovementioned seven POCs greatly increase the number of hydrazone-linked organic cages with determined crystal structures, as only four of them were previously solved by SCXRD. Moreover, this study may shed light on solving the difficulty in hydrazone-linked COF crystal growth and structure determination. Interestingly, these hydrazone-linked POCs are stable in water and can effectively remove various types of water pollutants from radionuclide waste, toxic heavy metal ions, and organic micropollutants. To the best of our knowledge, **HPOC-101** and **HPOC-401** are the first two examples of POC adsorbents for systematic removal of many kinds of these pollutants. This finding not only reveals that CR4ACHO can be regarded as an excellent molecular building block to construct versatile robust POCs but also broadens the application of POC materials in aqueous systems. Research on rational construction of robust calix[4]

 © 2021 The Author(s). Published by the Royal Society of Chemistry

Open Access Article. Published on 23 shtator 2021. Downloaded on 12.8.2025 2:07:18 e pasdites.
This article is licensed under a Creative Commons Attribution-NonCommercial 3.0 Unported Licence.

resorcinarene-based POCs and their practical applications by introducing hydrazide-containing ligands with functional groups is ongoing.

Data availability

Raw data are available upon request from the authors.

Author contributions

D. Y. and K. S. proposed the ideas and supervised the project. M. Y. performed the majority of the experiments. All authors contributed to the analysis and writing.

Conflicts of interest

There are no conflicts to declare.

Acknowledgements

This work was financially supported by the National Natural Science Foundation of China (22071244) and the Strategic Priority Research Program of the Chinese Academy of Sciences (XDB20000000).

References

1 T. Hasell and A. I. Cooper, *Nat. Rev. Mater.*, 2016, **1**, 16053.
2 M. Mastalerz, *Acc. Chem. Res.*, 2018, **51**, 2411–2422.
3 Y. Jin, Q. Wang, P. Taynton and W. Zhang, *Acc. Chem. Res.*, 2014, **47**, 1575–1586.
4 F. Beuerle and B. Gole, *Angew. Chem., Int. Ed.*, 2018, **57**, 4850–4878.
5 S. Huang, Z. Lei, Y. Jin and W. Zhang, *Chem. Sci.*, 2021, **12**, 9591–9606.
6 H. Wang, Y. Jin, N. Sun, W. Zhang and J. Jiang, *Chem. Soc. Rev.*, 2021, **50**, 8874–8886.
7 P. J. Waller, F. Gandara and O. M. Yaghi, *Acc. Chem. Res.*, 2015, **48**, 3053–3063.
8 K. Geng, T. He, R. Liu, S. Dalapati, K. T. Tan, Z. Li, S. Tao, Y. Gong, Q. Jiang and D. Jiang, *Chem. Rev.*, 2020, **120**, 8814–8933.
9 C. Gropp, T. Ma, N. Hanikel and O. M. Yaghi, *Science*, 2020, **370**, 424–431.
10 T. Hasell, H. Zhang and A. I. Cooper, *Adv. Mater.*, 2012, **24**, 5732–5737.
11 Q. Song, S. Jiang, T. Hasell, M. Liu, S. Sun, A. K. Cheetham, E. Sivaniah and A. I. Cooper, *Adv. Mater.*, 2016, **28**, 2629.
12 T. Tozawa, J. T. A. Jones, S. I. Swamy, S. Jiang, D. J. Adams, S. Shakespeare, R. Clowes, D. Bradshaw, T. Hasell, S. Y. Chong, C. Tang, S. Thompson, J. Parker, A. Trewin, J. Bacsa, A. M. Z. Slawin, A. Steiner and A. I. Cooper, *Nat. Mater.*, 2009, **8**, 973–978.
13 K. Acharyya and P. S. Mukherjee, *Angew. Chem., Int. Ed.*, 2019, **58**, 8640–8653.
14 G. Zhang and M. Mastalerz, *Chem. Soc. Rev.*, 2014, **43**, 1934–1947.
15 S. Ivanova, E. Koester, J. J. Holstein, N. Keller, G. H. Clever, T. Bein and F. Beuerle, *Angew. Chem., Int. Ed.*, 2021, **60**, 17455–17463.
16 P. Wagner, F. Rominger, W.-S. Zhang, J. H. Gross, S. M. Elbert, R. R. Schroeder and M. Mastalerz, *Angew. Chem., Int. Ed.*, 2021, **60**, 8896–8904.
17 B. Moosa, L. O. Alimi, A. Shkurenko, A. Fakim, P. M. Bhatt, G. Zhang, M. Eddaoudi and N. M. Khashab, *Angew. Chem., Int. Ed.*, 2020, **59**, 21367–21371.
18 C. Liu, K. Liu, C. Wang, H. Liu, H. Wang, H. Su, X. Li, B. Chen and J. Jiang, *Nat. Commun.*, 2020, **11**, 1047.
19 Z. Sun, P. Li, S. Xu, Z.-Y. Li, Y. Nomura, Z. Li, X. Liu and S. Zhang, *J. Am. Chem. Soc.*, 2020, **142**, 10833–10840.
20 H. Qu, Z. Huang, X. Dong, X. Wang, X. Tang, Z. Li, W. Gao, H. Liu, R. Huang, Z. Zhao, H. Zhang, L. Yang, Z. Tian and X. Cao, *J. Am. Chem. Soc.*, 2020, **142**, 16223–16228.
21 J. T. A. Jones, T. Hasell, X. Wu, J. Bacsa, K. E. Jelfs, M. Schmidtmann, S. Y. Chong, D. J. Adams, A. Trewin, F. Schiffman, F. Cora, B. Slater, A. Steiner, G. M. Day and A. I. Cooper, *Nature*, 2011, **474**, 367–371.
22 G. Zhang, O. Presly, F. White, I. M. Oppel and M. Mastalerz, *Angew. Chem., Int. Ed.*, 2014, **53**, 1516–1520.
23 P. Li, S. J. Xu, C. Y. Yu, Z. Y. Li, J. P. Xu, Z. M. Li, L. Y. Zou, X. B. Leng, S. Gao, Z. Q. Liu, X. Y. Liu and S. D. Zhang, *Angew. Chem., Int. Ed.*, 2020, **59**, 7113–7121.
24 N. Giri, C. E. Davidson, G. Melaugh, M. G. Del Pópolo, J. T. A. Jones, T. Hasell, A. I. Cooper, P. N. Horton, M. B. Hursthouse and S. L. James, *Chem. Sci.*, 2012, **3**, 2153–2157.
25 B. Mondal, K. Acharyya, P. Howlader and P. S. Mukherjee, *J. Am. Chem. Soc.*, 2016, **138**, 1709–1716.
26 T. P. Moneypenny II, N. P. Walter, Z. Cai, Y.-R. Miao, D. L. Gray, J. J. Hinman, S. Lee, Y. Zhang and J. S. Moore, *J. Am. Chem. Soc.*, 2017, **139**, 3259–3264.
27 G. Zhang, O. Presly, F. White, I. M. Oppel and M. Mastalerz, *Angew. Chem., Int. Ed.*, 2014, **53**, 5126–5130.
28 H. Ding, Y. Yang, B. Li, F. Pan, G. Zhu, M. Zeller, D. Yuan and C. Wang, *Chem. Commun.*, 2015, **51**, 1976–1979.
29 E. O. Pyzer-Knapp, H. P. G. Thompson, F. Schiffmann, K. E. Jelfs, S. Y. Chong, M. A. Little, A. I. Cooper and G. M. Day, *Chem. Sci.*, 2014, **5**, 2235–2245.
30 R. J. Kearsey, B. M. Alston, M. E. Briggs, R. L. Greenaway and A. I. Cooper, *Chem. Sci.*, 2019, **10**, 9454–9465.
31 M. W. Schneider, I. M. Oppel, H. Ott, L. G. Lechner, H.-J. S. Hauswald, R. Stoll and M. Mastalerz, *Chem. - Eur. J.*, 2012, **18**, 836–847.
32 C. Zhang, Z. Wang, L. Tan, T. L. Zhai, S. Wang, B. Tan, Y. S. Zheng, X. L. Yang and H. B. Xu, *Angew. Chem., Int. Ed.*, 2015, **54**, 9244–9248.
33 H. H. Duan, Y. W. Li, Q. F. Li, P. P. Wang, X. R. Liu, L. Cheng, Y. Yu and L. P. Cao, *Angew. Chem., Int. Ed.*, 2020, **59**, 10101–10110.
34 A. Avellaneda, P. Valente, A. Burgun, J. D. Evans, A. W. Markwell-Heys, D. Rankine, D. J. Nielsen, M. R. Hill, C. J. Sumby and C. J. Doonan, *Angew. Chem., Int. Ed.*, 2013, **52**, 3746–3749.

Open Access Article. Published on 23 shtator 2021. Downloaded on 12.8.2025 2:07:18 e pasdites.
This article is licensed under a Creative Commons Attribution-NonCommercial 3.0 Unported Licence.

35 X. Zhao, Y. Liu, Z.-Y. Zhang, Y. Wang, X. Jia and C. Li, *Angew. Chem., Int. Ed.*, 2021, **60**, 17904–17909.
36 Q. Wang, C. Zhang, B. C. Noll, H. Long, Y. Jin and W. Zhang, *Angew. Chem., Int. Ed.*, 2014, **53**, 10663–10667.
37 Q. Wang, C. Yu, C. Zhang, H. Long, S. Azarnoush, Y. Jin and W. Zhang, *Chem. Sci.*, 2016, **7**, 3370–3376.
38 S. Lee, A. Yang, T. P. Moneypenny II and J. S. Moore, *J. Am. Chem. Soc.*, 2016, **138**, 2182–2185.
39 C. Zhang, Q. Wang, H. Long and W. Zhang, *J. Am. Chem. Soc.*, 2011, **133**, 20995–21001.
40 J. L. Culshaw, G. Cheng, M. Schmidtmann, T. Hasell, M. Liu, D. J. Adams and A. I. Cooper, *J. Am. Chem. Soc.*, 2013, **135**, 10007–10010.
41 M. Liu, M. A. Little, K. E. Jelfs, J. T. A. Jones, M. Schmidtmann, S. Y. Chong, T. Hasell and A. I. Cooper, *J. Am. Chem. Soc.*, 2014, **136**, 7583–7586.
42 A. S. Bhat, S. M. Elbert, W. S. Zhang, F. Rominger, M. Dieckmann, R. R. Schroder and M. Mastalerz, *Angew. Chem., Int. Ed.*, 2019, **58**, 8819–8823.
43 E. Martinez-Ahumada, D. He, V. Berryman, A. Lopez-Olvera, M. Hernandez, V. Jancik, V. Martis, M. A. Vera, E. Lima, D. J. Parker, A. I. Cooper, I. A. Ibarra and M. Liu, *Angew. Chem., Int. Ed.*, 2021, **60**, 17556–17563.
44 Y. Jin, B. A. Voss, R. D. Noble and W. Zhang, *Angew. Chem., Int. Ed.*, 2010, **49**, 6348–6351.
45 S. Hong, M. R. Rohman, J. Jia, Y. Kim, D. Moon, Y. Kim, Y. H. Ko, E. Lee and K. Kim, *Angew. Chem., Int. Ed.*, 2015, **54**, 13241–13244.
46 M. W. Schneider, I. M. Oppel, A. Griffin and M. Mastalerz, *Angew. Chem., Int. Ed.*, 2013, **52**, 3611–3615.
47 S. Bera, K. Dey, T. K. Pal, A. Halder, S. Tothadi, S. Karak, M. Addicoat and R. Banerjee, *Angew. Chem., Int. Ed.*, 2019, **58**, 4243–4247.
48 T. Jiao, G. Wu, Y. Zhang, L. Shen, Y. Lei, C.-Y. Wang, A. C. Fahrenbach and H. Li, *Angew. Chem., Int. Ed.*, 2020, **59**, 18350–18367.
49 Z. Li, T. He, Y. Gong and D. Jiang, *Acc. Chem. Res.*, 2020, **53**, 1672–1685.
50 G. Zhang, Y.-l. Hong, Y. Nishiyama, S. Bai, S. Kitagawa and S. Horike, *J. Am. Chem. Soc.*, 2019, **141**, 1227–1234.
51 X. Wang, L. Chen, S. Y. Chong, M. A. Little, Y. Wu, W.-H. Zhu, R. Clowes, Y. Yan, M. A. Zwijnenburg, R. S. Sprick and A. I. Cooper, *Nat. Chem.*, 2018, **10**, 1180–1189.
52 J.-L. Lin, Z.-K. Wang, Z.-Y. Xu, L. Wei, Y.-C. Zhang, H. Wang, D.-W. Zhang, W. Zhou, Y.-B. Zhang, Y. Liu and Z.-T. Li, *J. Am. Chem. Soc.*, 2020, **142**, 9079.
53 S.-Y. Ding, M. Dong, Y.-W. Wang, Y.-T. Chen, H.-Z. Wang, C.-Y. Su and W. Wang, *J. Am. Chem. Soc.*, 2016, **138**, 3031–3037.
54 S. Mondal, B. Mohanty, M. Nurhuda, S. Dalapati, R. Jana, M. Addicoat, A. Datta, B. K. Jena and A. Bhaumik, *ACS Catal.*, 2020, **10**, 5623–5630.
55 H. Li, H. Zhang, A. D. Lammer, M. Wang, X. Li, V. M. Lynch and J. L. Sessler, *Nat. Chem.*, 2015, **7**, 1003–1008.
56 M. Wierzbicki, A. A. Glowacka, M. P. Szymanski and A. Szumna, *Chem. Commun.*, 2017, **53**, 5200–5203.
57 Z. Lin, T. J. Emge and R. Warmuth, *Chem. - Eur. J.*, 2011, **17**, 9395–9405.
58 H. Jedrzejewska, E. Wielgus, S. Kazmierski, H. Rogala, M. Wierzbicki, A. Wroblewska, T. Pawlak, M. J. Potrzebowski and A. Szumna, *Chem. - Eur. J.*, 2020, **26**, 1558–1566.
59 J. Koo, I. Kim, Y. Kim, D. Cho, I.-C. Hwang, R. D. Mukhopadhyay, H. Song, Y. H. Ko, A. Dhamija, H. Lee, W. Hwang, S. Kim, M.-H. Baik and K. Kim, *Chem*, 2020, **6**, 3374–3384.
60 K. Kobayashi and M. Yamanaka, *Chem. Soc. Rev.*, 2015, **44**, 449–466.
61 S. J. Dalgarno, S. A. Tucker, D. B. Bassil and J. L. Atwood, *Science*, 2005, **309**, 2037–2039.
62 E. J. Gosselin, C. A. Rowland and E. D. Bloch, *Chem. Rev.*, 2020, **120**, 8987–9014.
63 C. M. Kane, A. Banisafar, T. P. Dougherty, L. J. Barbour and K. T. Holman, *J. Am. Chem. Soc.*, 2016, **138**, 4377–4392.
64 Q. Zhang, L. Catti and K. Tiefenbacher, *Acc. Chem. Res.*, 2018, **51**, 2107–2114.
65 W.-Y. Pei, G. Xu, J. Yang, H. Wu, B. Chen, W. Zhou and J.-F. Ma, *J. Am. Chem. Soc.*, 2017, **139**, 7648–7656.
66 K. Su, W. Wang, B. Li and D. Yuan, *ACS Sustainable Chem. Eng.*, 2018, **6**, 17402–17409.
67 K. Su, W. Wang, S. Du, C. Ji, M. Zhou and D. Yuan, *J. Am. Chem. Soc.*, 2020, **142**, 18060–18072.
68 Y. Zhang, K. Su, Z. Hong, Z. Han and D. Yuan, *Ind. Eng. Chem. Res.*, 2020, **59**, 7247–7254.
69 K. Su, W. Wang, S. Du, C. Ji and D. Yuan, *Nat. Commun.*, 2021, **12**, 3703.
70 W. Wang, K. Su, E.-S. M. El-Sayed, M. Yang and D. Yuan, *ACS Appl. Mater. Interfaces*, 2021, **13**, 24042–24050.
71 G. J. Kleywegt and T. A. Jones, *Acta Crystallogr., Sect. D: Biol. Crystallogr.*, 1994, **50**, 178–185.
72 https://xray.bmc.uu.se/usf/.
73 pyWINDOW a Python package for structural analysis of discrete molecules with voids and windows. https://github.com/marcinmiklitz/pywindow.
74 S. Das, T. S. Herng, J. L. Zafra, P. M. Burrezo, M. Kitano, M. Y. Ishida, T. Y. Gopalakrishna, P. Hu, A. Osuka, J. Casado, J. Ding, D. Casanova and J. Wu, *J. Am. Chem. Soc.*, 2016, **138**, 7782–7790.
75 X.-S. Ke, T. Kim, Q. He, V. M. Lynch, D. Kim and J. L. Sessler, *J. Am. Chem. Soc.*, 2018, **140**, 16455–16459.
76 X.-Z. Li, L.-P. Zhou, L.-L. Yang, D.-Q. Yuan, C.-S. Lin and Q.-F. Sun, *J. Am. Chem. Soc.*, 2017, **139**, 8237–8244.
77 C. J. Pugh, V. Santolini, R. L. Greenaway, M. A. Little, M. E. Briggs, K. E. Jelfs and A. I. Cooper, *Cryst. Growth Des.*, 2018, **18**, 2759–2764.
78 A. L. Spek, *Acta Crystallogr., Sect. C: Struct. Chem.*, 2015, **71**, 9–18.
79 Y. He, S. Xiang and B. Chen, *J. Am. Chem. Soc.*, 2011, **133**, 14570–14573.
80 P. Li, Y. He, Y. Zhao, L. Weng, H. Wang, R. Krishna, H. Wu, W. Zhou, M. O'Keeffe, Y. Han and B. Chen, *Angew. Chem., Int. Ed.*, 2015, **54**, 574–577.

 © 2021 The Author(s). Published by the Royal Society of Chemistry

Open Access Article. Published on 23 shtator 2021. Downloaded on 12.8.2025 2:07:18 e pasdites.
This article is licensed under a Creative Commons Attribution-NonCommercial 3.0 Unported Licence.

81 P. Wei, X. He, Z. Zheng, D. He, Q. Li, J. Gong, J. Zhang, H. H. Y. Sung, I. D. Williams, J. W. Y. Lam, M. Liu and B. Z. Tang, *Angew. Chem., Int. Ed.*, 2021, **60**, 7148–7154.
82 J. Lue, C. Perez-Krap, M. Suyetin, N. H. Alsmail, Y. Yan, S. Yang, W. Lewis, E. Bichoutskaia, C. C. Tang, A. J. Blake, R. Cao and M. Schroeder, *J. Am. Chem. Soc.*, 2014, **136**, 12828–12831.
83 Z. Wang, N. Sikdar, S.-Q. Wang, X. Li, M. Yu, X.-H. Bu, Z. Chang, X. Zou, Y. Chen, P. Cheng, K. Yu, M. J. Zaworotko and Z. Zhang, *J. Am. Chem. Soc.*, 2019, **141**, 9408–9414.
84 Y. Jin, B. A. Voss, A. Jin, H. Long, R. D. Noble and W. Zhang, *J. Am. Chem. Soc.*, 2011, **133**, 6650–6658.
85 P. T. Smith, B. P. Benke, Z. Cao, Y. Kim, E. M. Nichols, K. Kim and C. J. Chang, *Angew. Chem., Int. Ed.*, 2018, **57**, 9684–9688.
86 S. Rojas and P. Horcajada, *Chem. Rev.*, 2020, **120**, 8378–8415.
87 X. Liu, H. Pang, X. Liu, Q. Li, N. Zhang, L. Mao, M. Qiu, B. Hu, H. Yang and X. Wang, *The Innovation*, 2021, **2**, 100076.
88 A. Alsbaiee, B. J. Smith, L. Xiao, Y. Ling, D. E. Helbling and W. R. Dichtel, *Nature*, 2016, **529**, 190–U146.
89 A. K. Mohammed, S. Usgaonkar, F. Kanheerampockil, S. Karak, A. Halder, M. Tharkar, M. Addicoat, T. G. Ajithkumar and R. Banerjee, *J. Am. Chem. Soc.*, 2020, **142**, 8252–8261.
90 S. Karak, K. Dey, A. Torris, A. Halder, S. Bera, F. Kanheerampockil and R. Banerjee, *J. Am. Chem. Soc.*, 2019, **141**, 7572–7581.
91 K. Dey, S. Mohata and R. Banerjee, *ACS Nano*, 2021, **15**, 12723–12740.